

1

2

3 **High-throughput generation of product profiles for**
4 **arabinoxylan-active enzymes from metagenomes**

5 Metagenome-derived AX-active enzymes product profiles

6

7

8 **Maria João Maurício da Fonseca^a, Zachary Armstrong^{b,*}, Stephen G. Withers^b,**

9 **Yves Briers^{a,#}**

10 ^a Department of Biotechnology, Ghent University, Ghent, Belgium.

11 ^b Department of Chemistry, University of British Columbia, Vancouver, Canada.

12

13

14

15

16 [#] Corresponding author: yves.briers@ugent.be

17 ^{*}Current affiliation: Department of Chemistry, The University of York, York, United Kingdom.

18

19

20

21 **Keywords:** arabinoxylan, enzyme discovery, metagenomics, substrate specificity, DSA-FACE

22

23 **Abstract**

24 Metagenomics is an exciting alternative to seek for carbohydrate-active enzymes from a range of
25 sources. Typically, metagenomics reveals dozens of putative catalysts that require functional
26 characterization for further application in industrial processes. High-throughput screening
27 methods compatible with adequate natural substrates are crucial for an accurate functional
28 elucidation of substrate preferences. Based on DNA sequencer-aided fluorophore-assisted
29 carbohydrate electrophoresis (DSA-FACE) analysis of enzymatic reaction products, we
30 generated product profiles to consequently infer substrate cleavage positions, resulting in the
31 generation of enzymatic degradation maps. Product profiles were produced in high-throughput
32 for arabinoxylan (AX)-active enzymes belonging to the glycoside hydrolase families GH43
33 (subfamilies 2 (MG43₂), 7 (MG43₇) and 28 (MG43₂₈)) and GH8 (MG8) starting from twelve
34 (arabino)xylo-oligosaccharides. These enzymes were discovered through functional metagenomic
35 studies of faeces from the North American beaver (*Castor canadensis*). This work shows how
36 enzyme loading alters the product profiles produced by all enzymes studied and gives insight into
37 AX degradation patterns revealing sequential substrate preferences of AX-active enzymes.

38

39 **Importance**

40 Arabinoxylan is mainly found in the hemicellulosic fractions of rice straw, corn cobs and rice
41 husk. Converting arabinoxylan into (arabino)xylo-oligosaccharides as added value products that
42 can be applied in food, feed, and cosmetics presents a sustainable and economic alternative for
43 the biorefinery industries. An efficient and profitable AX degradation requires a set of enzymes
44 with particular characteristics. Therefore, enzyme discovery and study of substrate preferences is
45 of utmost importance. Beavers, as consumers of woody biomass are a promising source of a
46 repertoire of enzymes able to deconstruct hemicelluloses into soluble oligosaccharides. High-

- 47 throughput analysis of oligosaccharide profiles produced by these enzymes will assist in the
- 48 selection of the most appropriate enzymes for the biorefinery.

49 **Introduction**

50 Metagenomic studies of the microbial communities associated with plant cell wall degraders
51 reveal a large number of gene sequences coding for potential carbohydrate-active enzymes
52 (CAZymes) (1). Accurate functional analysis of new CAZymes must accompany this continuous
53 discovery at the genomic level. Such newly functionally validated enzymes can be applied in the
54 biorefinery industry and/or for further protein engineering (2-5). Glycoside hydrolases (GHs) that
55 cleave polysaccharide main chains and/or substituents can have complex substrate preferences,
56 often showing multi-substrate specificities (6-9). These substrate preferences are often also
57 dependent on main chain substituents. Consequently, the degradation of complex carbohydrate
58 polymers often requires synergistic or combinatorial action of multiple enzymes. Tedious
59 techniques, long analysis times, demanding hands-on assays, specialised equipment and lack of
60 appropriate representative substrates contribute to the existing gap between enzyme discovery
61 and functional characterization (10). Accordingly, high-throughput (HT) techniques that can deal
62 with a large number of metagenome-derived putative enzymes and that can give an insight into
63 the substrate specificities of unannotated enzymes in a relatively short time are required (11).
64 DNA sequencer-aided fluorophore-assisted carbohydrate electrophoresis (DSA-FACE) offers an
65 interesting approach to study the substrate specificities of CAZymes, primarily due to the
66 possibility to use substrates that represent the natural carbohydrates instead of artificial aryl
67 glycoside substrates like *p*-nitrophenyl- and 4-methylumbelliferyl-derivatives (12). In fact, the
68 latter substrate derivatives may mask the real enzymatic substrate specificity due to, for example,
69 steric differences in comparison to the natural oligosaccharides. DSA-FACE has shown
70 outstanding oligosaccharide resolution and sensitivity (a detection limit ranging from 38 to 55
71 pM for the substrates studied), short hands-on time and analysis time (13). In addition, DSA-

72 FACE allows analysis of the substrate specificities in HT when using multiple parallel capillaries
73 as in standard capillary sequencing devices.

74 In this work we focus on arabinoxylan (AX) which is a hemicellulosic polysaccharide that may
75 contain a range of substitutions including α -L-arabinofuranosyl, α -D-glucuronic acid, 4-O-
76 methyl- α -D-glucuronic acid, α -D-galactopyranose and ferulic acid residues, depending on the
77 source (14). Deconstruction of AX by GHs leads to useful sugars for the production of
78 bioethanol, food and nutraceutical added-value products such as xylitol (15-18) and prebiotics
79 (19-23). GHs with diverse substrate specificities for the degradation of complex AX structures
80 are being discovered continuously and annotated in the various protein databases (24). The
81 carbohydrate-active enzymes database (CAZy) classifies GHs into families according to amino
82 acid sequence similarity (25). Although structural similarity often correlates with enzyme
83 substrate specificity, the CAZy family division cannot always be used to predict enzyme
84 substrate specificity because of the different specificities assigned per GH family. Additionally,
85 up to now only approximately 1% of the annotated GHs in CAZy have been experimentally
86 characterized (25). Due to the abundance of GH43 members and the large substrate specificity
87 variety found within this family, the GH43 family was further divided into subfamilies on the
88 basis of sequence analyses, suggesting that the correlation between functional annotation of the
89 enzyme and subfamily assignment is more accurate (26). The GH43 family subdivision and
90 analysis relies on computational and experimental data, which are mainly based on synthetic
91 substrates such as *p*-nitrophenyl (*p*NP) monosaccharides. To obtain a more accurate
92 understanding of the substrate specificity of AX-active enzymes, we have recently used DSA-
93 FACE to analyze the hydrolysates of AX-active enzymes with natural representative
94 (arabino)xylo-oligosaccharides ((A)XOS) (13). In this work, DSA-FACE is used to elucidate
95 substrate specificities of enzymes derived from metagenomic studies on the North American

96 beaver (*Castor canadensis*) fecal microbiome (27). Three genes belonging to uncharacterized or
97 poorly characterized subfamilies 2, 7 and 28 of GH43 and one from GH8 that were identified in
98 active fosmids were shown to be active on AX by preliminary functional screening tests with aryl
99 glycosides and/or high-performance anion-exchange chromatography with pulsed amperometric
100 detection (HPAEC-PAD) (27) (Figure 1). To gain further insight into AX degradation patterns by
101 the aforementioned enzymes, we introduce DSA-FACE product profiles and associated
102 sequential degradation maps for a convenient representation of the activity(ies) of each enzyme
103 on twelve (A)XOS substrates. By implementing DSA-FACE product profiles, we reveal the
104 preferred substrate cleavage sites by a GH43₂₈ member, the modular specificity of a GH43₂ –
105 GH8 enzyme and the dependence of the enzymatic activity of a GH43₇ member on the activity of
106 the aforementioned GH43₂ – GH8 enzyme.

107

108 **Results**

109 *DSA-FACE allows rapid evaluation of product profiles produced by metagenome-derived AX-*
110 *active enzymes*

111 In this study, we have used DSA-FACE to set up product profiles for three newly-discovered
112 enzymes of the GH43 family active on AX. These enzymes were identified through a preceding
113 metagenomic analysis of the North American beaver (*Castor canadensis*) fecal microbiome (27).
114 The first selected enzyme (MG43₂₈) contains a GH43 subfamily 28 domain. The second enzyme
115 (MG43₂₋₈) is a modular enzyme composed of a GH43 subfamily 2 and a GH8 domain. To
116 differentiate the specificities of each domain, we have also set up product profiles produced by
117 two mutated variants, in which the respective domains are inactivated by mutagenesis of the
118 catalytic acid residue (27), resulting in MG43₂ and MG8, respectively (Table 1). The third
119 enzyme MG43₇ comprises a single domain assigned to GH43 subfamily 7. These enzymes were

120 selected because of the limited characterization for these subfamilies. An initial analysis of these
121 enzymes with chromogenic substrates and HPAEC-PAD confirmed that they have AX-acting
122 activities as summarized in Table 1. The initial low expression yields of MG43₂₋₈, MG43₂ and
123 MG43₇ were optimized by variation of expression strains, growth temperature, induction and
124 purification protocols (Table 2). Eluted fractions from the different expressions/purifications
125 containing the desired protein were pooled for further analysis.

126 DSA-FACE product profiles are a qualitative representation of the carbohydrates present after
127 enzymatic reactions with different (A)XOS (Figure 2A). Twelve oligosaccharides (5 XOS, 7
128 AXOS) are used in these enzymatic reactions. Reaction hydrolysates are then analyzed with
129 DSA-FACE. The output of DSA-FACE are electropherograms that need to be interpreted by
130 referencing to (A)XOS standards to reveal the identity of the resulting products. Peak areas are
131 quantified and normalized to calculate the relative conversion of each substrate and relative
132 proportion of the products. This has been exemplified in Figure 2B for a previously characterized
133 α -L-arabinofuranosidase from *Bifidobacterium adolescentis* (BaAXH-d3) (13). Alpha-L-
134 arabinofuranosidases are classified into arabinoxylan arabinofuranohydrolases (AXH) that
135 hydrolyze the O-2 and/or O-3 arabinofuranosyl monomers from the doubly substituted xyloses
136 (AXH-d2, AXH-d3, AXH-d2,3) or from the mono substituted xyloses (AXH-m2, AXH-m3,
137 AXH-m2,3). To simplify the representation of enzymatic substrate preferences, we introduce
138 here product profiles with a fixed color code instead of electropherograms as the final DSA-
139 FACE outcome. Substrate conversions are easily observed in the product profiles by a color
140 change. Accordingly, there is only a color change in the case of A²⁺³XX and XA²⁺³XX for
141 BaAXH-d3. Next to the product profiles, degradation maps highlighting cleavage positions for
142 the different (A)XOS tested are elaborated to assist in evaluating enzyme substrate preferences.

143

144 *Different product profiles for increasing MG43₂₈ concentrations*

145 Purified MG43₂₈ was tested against the panel of five XOS and seven AXOS using four different
146 enzyme concentrations (0.3 – 1 – 6 – 32 μM). The product profiles of MG43₂₈ show diverse
147 hydrolytic products which change depending on the enzyme concentration (Figure 3). At the
148 lowest concentration tested (0.3 μM) MG43₂₈ completely removes an *O*-2 arabinose from a non-
149 reducing end singly substituted xylose, i.e. A²XX to X₃ (AXH-m2 activity). In addition, at
150 concentrations at or above 0.3 μM MG43₂₈ both *O*-2 and *O*-3 arabinoses are partially removed
151 from the non-reducing end doubly substituted xylose of A²⁺³XX, resulting in X₃ (AXH-d2,3
152 activity), but higher concentrations (6 μM) are needed for a full conversion. The internal *O*-2
153 arabinose from XA²XX is only removed from 1 μM and even at the highest concentration studied
154 (32 μM) MG43₂₈ is not able to remove *O*-2 and *O*-3 arabinoses from XA²⁺³XX, indicating that
155 the internal single/double arabinose substitutions are less accessible for hydrolysis. Removal of
156 the *O*-3 arabinoses from A³XX and XA³XX (AXH-m3 activity), resulting in X₃ and X₄,
157 respectively, is observed from 1 μM MG43₂₈. MG43₂₈ thus exerts diverse arabinofuranosidase
158 specificities with the best conversion of A²XX. Xylanolytic activity is visible at concentrations at
159 or above 1 μM as well, with a preference for the longest xylo-oligosaccharide tested (X₆). Also,
160 AXOS with removed arabinoses are further partially degraded (e.g. XA³XX is converted to X₂
161 and X₄).

162

163 *The product profiles for MG43₂₋₈ are the sum of the product profiles of its respective domains*

164 Enzymatic reactions with purified MG43₂, MG8 and MG43₂₋₈ were performed. The product
165 profiles in Figure 4 demonstrate that MG43₂ is a β-xylosidase and MG8 is a reducing end xylose-
166 releasing exo-oligoxyylanase (Rex). At a concentration of 3 μM, MG43₂ partially converts XOS
167 into X₂. It seems there are more structural hindrances or product inhibition in comparison to MG8

168 based on the slower observed degradation rate. MG43₂ does hydrolyze the non-reducing xylose
169 monomers from XA²XX, XA³XX and XA²⁺³XX (Figure 4A) but not the non-reducing arabinose
170 substituted xylose monomers (A²XX, A³XX and A²⁺³XX). At a concentration of 3 μM MG8 fully
171 converts X₃, X₄ and X₅ to X₂, but we did not observe visible conversion of X₂ to X. However, X₆
172 seems to be more slowly converted to X₂ due to possible hindrances in accommodating long XOS
173 into MG8 catalytic subsites or due to product inhibition, indicating a preference for smaller XOS.
174 As typical for Rex enzymes, MG8 requires two non-substituted xyloses from the reducing end to
175 hydrolyse the reducing end xylose (28, 29). This is observed when the reducing end xylose
176 monomer is hydrolysed from A²XX, A³XX, A²⁺³XX, XA²XX, XA³XX and XA²⁺³XX but not
177 from A³X. We also evaluated different concentrations for MG8 (0.2, 0.8, 3 and 17 μM) (Figure
178 S1). Notably, at the minimum MG8 concentration tested (0.2 μM) only X₃ to X₆ were partially
179 hydrolysed into smaller dp XOS, showing the preference for XOS over AXOS by MG8. At
180 concentrations from 0.8 to 17 μM, MG8 shows the same product profiles as the ones performed
181 with 3 μM enzyme (Figure 4).

182 At concentrations of 3 μM MG43₂₋₈ displays the sum of both β-xylosidase and Rex activities
183 (Figure 4). When we evaluated MG43₂₋₈ at a higher concentration (17 μM), MG43₂₋₈ also
184 exhibited α-L-arabinofuranosidase activity when hydrolyzing the mixture of XA²XX and XA³XX
185 into A²X, A³X and X₂ (Figure S2). This is likely performed by the MG43₂ domain since 17 μM
186 MG8 did not show α-L-arabinofuranosidase activity on any of the substrates tested and 3 μM
187 MG43₂ showed a small amount of α-L-arabinofuranosidase activity on A³X but not on A³XX or
188 XA³XX (Figure 4).

189

190 *Product profiles of MG43₇ change with increasing MG43₇ concentration and in the presence of*

191 *MG43₂₋₈/MG43₂/MG8*

192 MG43₇ activity was only detected at the highest concentration tested (38 μM). MG43₇ showed a
193 xylanase activity on X₄, X₅ and X₆ (Figure S3). Yet, when enzymatic reactions were performed
194 with 8 μM MG43₇ in the presence of 3 μM MG43₂₋₈, A³X is converted to X₂, showing an
195 additional AXH-m3 activity, which does not happen when enzymatic reactions are performed
196 with the same concentrations of MG43₂₋₈ or MG43₇ alone (Figure 5). X₂ and X₃ can also be
197 observed after enzymatic reactions with 8 μM MG43₇ in the presence of 3 μM MG43₂₋₈ and
198 A³XX or XA³XX, again showing additional AXH-m3 activity. Notably, *O*-2 arabinofuranosyl
199 substitutions are not a substrate since A²XX is not further hydrolyzed to X₂. When enzymatic
200 reactions were performed with elevated concentrations (38 μM MG43₇ in the presence of 17 μM
201 MG43₂₋₈) and A³X, the end product was again X₂, showing no further hydrolysis, but when the
202 same concentrations were tested against A²XX, A²X and X₂ appeared as reaction products
203 (Figure S2).

204 To discriminate whether the additional AXH-m3 or AXH-m2 activity that appears when
205 combining MG43₇ and MG43₂₋₈, comes from either MG43₇ or MG43₂₋₈, we investigated again
206 the activity of MG43₇ in the presence of the derivatives of MG43₂₋₈ in which one domain was
207 inactivated by mutation (MG43₂ and MG8). When A³X reacted with 8 μM MG43₇ and 3 μM
208 MG43₂ (Figure S4), approximately 50% A³X was converted to X₂. The same reaction but in
209 combination with 3 μM MG8 also resulted in a minor fraction of X₂ (Figure S1). These data
210 indicate that the AXH-m3 activity does indeed result from MG43₇. This finds further support as
211 also AXH-m3 activity is detected in both cases when a mixture of A²XX/A³XX reacts with
212 MG43₇ in the presence of either MG43₂ (Figure S4) or MG8 (Figure S1). Likely MG43₇ has a
213 preference for non-reducing *O*-3 substituted xyloses since 8 μM MG43₇ and 3 μM MG8 do not
214 hydrolyze XA³XX further into X₂. These findings are consistent with the previously identified
215 arabinofuranosidase activity of MG43₇ on A³X detected by HPAEC-PAD (27). In sum, the scans

216 indicate that MG43₇ shows AXH-m₃ activity on small *O*-3 arabinose substituted AXOS (A³X
217 and A³XX) in the presence of MG43₂₋₈, and xylanase activity at elevated concentrations.
218

219 **Discussion**

220 Functional metagenomic studies of the beaver fecal microbiome revealed enzymes from
221 subfamilies 2, 7 and 28 of the GH43 CAZy family. Whereas subfamily 2 has two characterized α -
222 L-arabinofuranosidases from *Chitinophaga pinensis* DSM2588 and *Mucilaginibacter mallensis*
223 MP1X4 (3, 30), subfamilies 7 and 28 have no characterized enzymes to date. Activity on CMU-X
224 indicated that MG43₂₈ is a β -xylosidase (27). However, the MG43₂₈ product profiles reveal that
225 MG43₂₈ is able to hydrolyze all (A)XOS substrates except XA²⁺³XX, showing xylanase, AXH-
226 m_{2,3} and AXH-d_{2,3} activities. We cannot confirm if the observed xylanase activity is due to
227 endo- or sequential exo-xylanase activity. If MG43₂₈ acts as a β -xylosidase it would be expected
228 that X₂ is also degraded to X, which does not seem to happen even at the highest concentration
229 tested. Though, monomeric xylose cannot be detected by DSA-FACE. Similarly, GH43
230 *PcAxy43A* from *Paenibacillus curdlanolyticus* (GH43 subfamily 35) is also unable to hydrolyze
231 XA²⁺³XX and shows endo-xylanase, β -xylosidase, AXH-d_{2,3} and AXH-m_{2,3} activities in a
232 single catalytic domain (31), but the presence of both exo- and endo-activity in a single enzyme
233 can be considered unusual. Ara 1 isolated from barley malt also has both AXH-m_{2,3} and AXH-
234 d_{2,3} activities and a four times higher enzyme concentration is needed for conversion of
235 XA²⁺³XX into X₄ than for conversion of A²⁺³XX (32). Besides a N-terminal MG43₂₈ GH43
236 domain, a C-terminal discoidin domain has been identified using the Conserved Domain
237 database. This discoidin domain has putative lectin-like properties, binding carbohydrates (33).
238 To unravel how MG43₂₈ deals with such a variety of substrates, the influence of this C-terminal
239 domain on the observed multiple activities may be investigated. A blastp analysis of MG43₂₈

240 against all GH43 CAZy family characterized sequences (182 characterized sequences out of
241 16250) revealed an enzyme from *Belliella baltica* DSM 15883 (accession number: AFL85801.1)
242 as the most similar sequence (E-value 5×10^{-10} with 45% query cover and 25% percentage
243 identity). This enzyme is annotated in GH43 subfamily 31 of the CAZy database and was
244 identified as a β -D-galactofuranosidase in the study of (3). The endo-1,4- β -xylanase from an
245 uncultured bacterium URE4 (accession number: ACM91046.1) shows the maximum query cover
246 of 85% (E-value: 1×10^{-4} , percentage identity: 23%). This enzyme is annotated in subfamily 29 of
247 the CAZy database. These relatively low similarities spread over different subfamilies emphasize
248 the need for detailed analyses of the substrate specificity as done here for MG43₂₈.
249 The substrate preferences of MG43₂₋₈, MG43₂, MG8, and MG43₇ in the presence of MG43₂₋₈
250 were previously analyzed by HPAEC-PAD upon enzymatic reactions with 0.5 μ M purified
251 enzyme and 4 mM A³X, A²XX and a mixture of XA²XX and XA³XX (27). At the conditions
252 tested MG43₂, MG8, and MG43₇ showed β -xylosidase, Rex and AXH-m3 activities, respectively.
253 Due to the limited HT capacity of HPAEC-PAD, a restricted number of substrates were tested,
254 omitting doubly substituted XOS, for example. The minor α -L-arabinofuranosidase activity of the
255 MG43₂ β -xylosidase against A³X indicates MG43₂ shows both β -xylosidase and AXH-m3
256 activities at concentrations higher than 3 μ M. Bifunctional β -xylosidase and α -L-
257 arabinofuranosidase activities have already been reported before in the GH43 CAZy family but
258 not yet in subfamily 2. It seems these enzymes can accommodate both xylose and arabinose units
259 in their active sites not only due to obvious structural similarities between arabinose and xylose
260 sugars, but also due to rotations on the α -arabinose linkage to xylose that can resemble a β -xylose
261 linkage in the main chain (34, 35). Accordingly, it can be questioned whether MG43₂ is actually
262 bifunctional or misrecognizes the substrate, which can be observed at an elevated enzyme
263 concentration.

264 Xylanolytic activity of MG43₂-8 and MG43₂ against X₂ remains ambiguous. DSA-FACE is not
265 able to detect xylose and can thus not detect possible X₂ degradation. Previous HPAEC-PAD
266 analyses show that X₂ was not hydrolyzed by MG43₂-8 and MG43₂ (27). In accordance with
267 these results, MG43₂-8 and MG43₂ were also not active against chromogenic pNP-X. However,
268 MG43₂-8 and MG43₂ showed activity with fluorogenic CMU-X, suggesting X₂ xylanolytic
269 activity. This discrepancy may be explained by the higher sensitivity when using fluorogenic
270 substrates. In sum, if MG43₂-8 and MG43₂ can hydrolyze X₂, it will be at maximum with a low
271 activity. This contrasts to many GH43 β -xylosidases that digest X₂ (36). Yet, β -xylosidases such
272 as XylB from *Bifidobacterium adolescentis* that prefer longer dp XOS over X₂ have also been
273 reported (37).

274 DSA-FACE demonstrated a strict Rex substrate specificity for MG8 and showed complete
275 substrate conversion at the maximum concentration tested. Up to now there are only four GH8
276 Rex enzymes characterized in the CAZy database, including enzymes from *Bacillus halodurans*
277 (38), *Bifidobacterium adolescentis* (39), *Bacteroides intestinalis* (40) and *Paenibacillus*
278 *barcinonensis* (29). MG8 shows a typical Rex activity (as the characterized Rex enzymes listed
279 above): MG8 does not hydrolyze pNP-X, is active on XOS with dp 3 to 6 and has a preference
280 for short dp XOS (41). Similar to Rex8A from *Paenibacillus barcinonensis*, which was the first
281 one tested against branched oligosaccharides (MeGlcA decorated xylooligomers), MG8 is able to
282 hydrolyze the reducing end xylose of branched AX-oligosaccharides. Notably, the *rex8A* gene
283 from *Bacteroides intestinalis* is located downstream a *xyl3A* gene, which encodes a β -xylosidase.
284 The X₂ generated by Rex8A is therefore hydrolyzed by the Xyl3A β -xylosidase. This is not the
285 case for MG43₂-8 as both MG43₂ and MG8 cannot efficiently hydrolyze X₂ as shown here and
286 before with HPAEC-PAD. β -Xylosidases such as MG43₂, and Rex such as MG8 which have low
287 or no X₂ hydrolytic activity are interesting for the incomplete degradation of AX into X₂. X₂ has

288 been demonstrated to be the most efficient prebiotic in terms of promoting a higher growth of
289 *Bifidobacterium* and *Lactobacillus* strains among the xylose polymers and to present an increased
290 sweetness power in comparison to sucrose (42).

291 MG43₇ shows a unique substrate specificity pattern, requiring the presence of MG43₂-
292 8/MG43₂/MG8 for activity. In fact, the MG43₂-8 and MG43₇ coding sequences were identified in
293 the same operon, already suggesting a natural synergy between these two enzymes. Notably,
294 MG43₇ only handles *O*-3 arabinofuranosyl substitutions of rather small AXOS. Previously a
295 GH43₁₈ metagenome-derived enzyme also showed a single preference for A³X from the (A)XOS
296 studied (13). At higher enzyme concentrations MG43₇ shows xylanase (either endo- or exo-
297 xylanase activity as discussed for MG43₂₈) activity on higher dp XOS and AXH-d2 activity on
298 internal arabinose substituted xyloses. Further investigation should be made to understand such
299 particular substrate recognition by MG43₇ and GH43₁₈.

300 It is worth noting that our study provides detailed insights into substrate preferences but not into
301 kinetics. Overnight reactions were performed, but often incomplete conversions were observed.
302 Similar observations of incomplete conversions were observed before with AX-acting enzymes
303 (31, 43-45). This may either indicate low rates, enzyme death and/or product inhibition. The
304 latter is less likely to be an issue in natural systems where other enzymes further convert the
305 product from the first reaction. Yet, product inhibition is highly relevant in industrial applications
306 where high substrate concentrations are used. Consequently, enzymes are either selected based on
307 low product inhibition levels (46, 47), or their crystal structure is determined to unravel the
308 structural basis of product inhibition, giving rise to opportunities for protein engineering to
309 release or reduce product inhibition (48).

310 In conclusion, DSA-FACE enables a HT analysis of enzymatic substrate preferences of AXOS-
311 acting enzymes in a relatively short experimental and analysis time. Thanks to the HT nature of

312 the approach, by performing enzymatic reactions at different enzyme concentrations, different
313 (A)XOS structures can be ranked as preferred substrates and sequential enzymatic cleavages can
314 be determined. This approach allowed us to create degradation maps for five metagenome-
315 derived enzymes for twelve different (A)XOS substrates. The knowledge of the exact substrate
316 preferences is undoubtedly essential to achieve either desired hydrolysis products (e.g. prebiotics)
317 or to come to a full hydrolysis. Finally, given the variety, promiscuity and flexible substrate
318 preferences of the majority of carbohydrate active enzymes, DSA-FACE may be explored for
319 other activities rather than (arabino)xylanolytic activities.

320

321 **Materials and methods**

322 *Expression and purification of metagenome-derived enzymes*

323 pET28 plasmids containing the enzyme DNA sequences were obtained as described previously
324 (27). Chemically competent *Escherichia coli* TOP10 and *E. coli* BL21 (DE3), *E. coli* BL21
325 CodonPlus (DE3) or *E. coli* ArcticExpress strains prepared according to the rubidium chloride
326 method were transformed with these plasmids.

327 Table 2 gives an overview of the enzyme expression conditions obtained after preceding
328 optimization steps. For optimal aeration, Erlenmeyer flasks exceeding at least four times the
329 expression volume were used. The different expression hosts were grown at indicated
330 temperatures in lysogeny broth (LB) with appropriate antibiotics until reaching an OD₆₀₀ of
331 approximately 0.6 followed by isopropyl β-D-1-thiogalactopyranoside (IPTG) induction. LBE-
332 5052 auto-induction medium consisted of 1% tryptone, 0.5% yeast extract, 40 mM K₂HPO₄, 10
333 mM KH₂PO₄, 50 mM NH₄Cl, 5 mM Na₂SO₄, 2 mM Mg₂SO₄, 0.5% glycerol, 0.05% glucose,
334 0.2% lactose, 50 μg/mL kanamycin and trace metals mix (50 μM FeCl₃, 20 μM CaCl₂, 10 μM
335 MnCl₂, 10 μM ZnSO₄, 2 μM CoCl₂, 2 μM CuCl₂, and 2 μM NiCl₂).

336 Cells were harvested by centrifugation at 3100 x g for 30 min at 4 °C. Pellets were then
337 suspended in 1/25 of the original volume in equilibration buffer for metal affinity
338 chromatography (see below) and 1 mg/mL lysozyme and incubated on ice for 30 min. After three
339 freeze-thaw cycles, sonication was performed on ice (3 x 30 s with 30 s interval, 40% amplitude).
340 Cell debris were removed by centrifugation at 20000 x g for 30 min at 4 °C and resulting
341 supernatants were clarified by filtration with a 0.45 µm filter. Purifications by metal affinity
342 chromatography were performed either with His GraviTrap columns (GE Healthcare) or HisPur
343 Ni-NTA Superflow agarose (Thermo Fisher Scientific). The manufacturer's protocols were
344 followed in both cases with the exception for the latter that the sample-resin incubation time was
345 extended to 1 h and buffers used were modified (20 mM sodium phosphate 500 mM NaCl 20
346 mM imidazole pH 7.4 as equilibration buffer, 20 mM sodium phosphate 500 mM NaCl 50 mM
347 imidazole pH 7.4 as wash buffer and 20 mM sodium phosphate 500 mM NaCl 500 mM
348 imidazole pH 7.4 as elution buffer).
349 Eluted samples were diluted with reducing sample buffer, boiled for 5 min and analyzed by 12%
350 SDS-Page (Roti®-Mark standard from Carl Roth was used). Fractions containing the protein of
351 interest were then dialyzed against 20 mM HEPES-NaOH buffer pH 7.0 and 300 mM NaCl,
352 pooled and concentrated with Vivaspin concentrators when necessary. Dialysis was done with
353 Slide-A-Lyzer™ MINI Dialysis Devices, 3.5K MWCO (Thermo Fisher Scientific) or with
354 SERVAPOR® dialysis tubing, MWCO 12000-14000 RC, diameter 16 mm. Protein
355 concentrations were measured with the Abs280nm app of the DeNovix DS-11 series
356 spectrophotometer. Extinction coefficients were calculated with the ProtParam tool (Expasy).
357
358
359

360 *Enzymatic reactions of metagenome-derived enzymes with (A)XOS*
361 Metagenome-derived enzymes were tested against (A)XOS (Figure 6) supplied by Megazyme
362 (Megazyme International Ireland, Bray, Ireland), which have a minimum purity of 95% except
363 for the mixture of A²XX and A³XX, which has a minimum purity of 90%, and for XA²⁺³XX
364 which has a minimum purity of 85%. Enzymatic reactions with a total volume of 100 μ L (or in
365 50 μ L to achieve desired enzyme concentration when there was only a limited enzyme volume
366 available) in a 96-well plate contained 0.2-38 μ M enzyme, 10 μ M (A)XOS, 50 mM HEPES-
367 NaOH 50 mM NaCl pH 7.0. Mineral oil (30-50 μ l) was used to avoid evaporation from the 96-
368 well plate during enzymatic reaction (Figure 7). Substrate and enzyme blanks, where enzyme and
369 substrate (respectively) were replaced by the corresponding buffer, have been added. Some
370 repetitions of reactions were performed in a 1.5 mL Eppendorf for reasons of simplicity.
371 Enzymatic reactions were incubated at 37 °C and 750 rpm in a Thermomixer comfort
372 (Eppendorf). The number of replicates done per enzyme/substrate combination is given in Table
373 S1. After 22 h, reactions were stopped by incubation at 80 °C for 30 min.

374

375 *Analysis of enzymatic reaction hydrolysates by DSA-FACE*

376 Reaction hydrolysates were diluted 10-fold with ultrapure water and 10 μ L were lyophilized.
377 Carbohydrates present in the lyophilized fraction were then derivatized with 8-aminopyrene-
378 1,3,6-trisulfonic acid trisodium salt (APTS) by reductive amination as in (13). Afterwards,
379 samples were quenched by diluting the reactions 200-fold with ultrapure water. Ten μ L of
380 derivatized hydrolysate was analyzed by the Applied BiosystemsTM 3130 Genetic Analyzer with
381 36 cm capillaries filled with Applied BiosystemsTM POP-7TM polymer as in (13) (Figure 7).
382 Through DSA-FACE electropherograms the carbohydrates before and after enzymatic reactions
383 are identified by comparison to standards. Xylose and arabinose monomers are not detected by

384 DSA-FACE as they fall into the DSA-FACE noise region due to their high electrophoretic
385 mobility. Since A^2X , $A^{2+3}X$, XA^2X , XA^3X and $XA^{2+3}X$ standards are not commercially available,
386 they were identified by comparison between the electrophoretic mobilities of the hydrolysates,
387 the electrophoretic mobilities of the available standards and based on spiking experiments (Figure
388 S5 and Figure S6). Previously it was seen that AXOS with dp z present an electrophoretic
389 mobility between XOS with dp z-1 and z showing an increased electrophoretic mobility in
390 comparison with XOS with the same dp. For example, A^2XX and A^3XX are therefore expected to
391 have an electrophoretic mobility in between X_3 and X_4 (13).

392

393 *DSA-FACE product profiles*

394 DSA-FACE product profiles were made with the excel graph function. Peak areas were collected
395 with the GeneMapper® Software Version 4.0. DSA-FACE peak area reproducibility is dependent
396 on the amount of labeled carbohydrate injected in each run, which may vary due to the
397 electrokinetic injection mechanism of the 3130 Genetic Analyzer. Intrinsic carbohydrate
398 electrophoretic mobilities affect the amount of sample injected by the electrokinetic mechanism
399 (49). Therefore peak areas are corrected by dividing the hydrolysate peak areas by the peak area
400 of the blank with same (A)XOS structure. When this AXOS was not one of the standard AXOS,
401 the peak area of an AXOS with the same dp is taken. The average of the corrected peak areas is
402 then taken for the DSA-FACE product profiles. To normalize all peak areas obtained for the
403 same enzyme but different enzyme concentrations and substrates, the largest peak area (or the
404 largest sum of the carbohydrate peak areas when more peaks are present in an hydrolysate) is
405 taken as the maximum amount of carbohydrate possibly found in a hydrolysate. All product
406 profiles revealed by DSA-FACE are summarized in Table S2.

407

408 *Data availability*

409 GenBank accession numbers for the enzyme DNA sequences 12_H03-13 (MG43₂₋₈), 12_H03-12
410 (MG43₇), and 12_J03-18 (MG43₂₈) (Table 1) are [MT603581](#), [MT603582](#) and [MT603583](#),
411 respectively.

412

413 **Acknowledgments**

414 We thank Ghent University (BOF Start Grant) and the Natural Sciences and Engineering
415 Research Council of Canada for the financial support to perform this work.

416

417 **References**

- 418 1. Hess M, Sczyrba A, Egan R, Kim T-W, Chokhawala H, Schroth G, Luo S, Clark DS,
419 Chen F, Zhang T, Mackie RI, Pennacchio LA, Tringe SG, Visel A, Woyke T, Wang Z,
420 Rubin EM. 2011. Metagenomic discovery of biomass-degrading genes and genomes from
421 cow rumen. *Science* 331:463-467.
- 422 2. Armstrong Z, Mewis K, Strachan C, Hallam SJ. 2015. Biocatalysts for biomass
423 deconstruction from environmental genomics. *Current Opinion in Chemical Biology*
424 29:18-25.
- 425 3. Helbert W, Poulet L, Drouillard S, Mathieu S, Loiodice M, Couturier M, Lombard V,
426 Terrapon N, Turchetto J, Vincentelli R, Henrissat B. 2019. Discovery of novel
427 carbohydrate-active enzymes through the rational exploration of the protein sequences
428 space. *Proceedings of the National Academy of Sciences of the United States of America*
429 116:10184-10185.

- 430 4. Chaturvedi T, Torres AI, Stephanopoulos G, Thomsen MH, Schmidt JE. 2020.
431 Developing process designs for biorefineries-definitions, categories, and unit operations.
432 *Energies* 13:22.
- 433 5. Villota EM, Dai Z, Lu Y, Yang B. 2020. Enzymes for cellulosic biomass hydrolysis and
434 saccharification, p 283-326. *In* Vertès AA, Qureshi N, Blaschek HP, Yukawa H (ed),
435 *Green energy to sustainability: strategies for global industries*. John Wiley & Sons Ltd.
- 436 6. Khandeparker R, Numan MT. 2008. Bifunctional xylanases and their potential use in
437 biotechnology. *Journal of industrial microbiology&biotechnology* 35:635-644.
- 438 7. Lee K-T, Touthik SH, Baek J-Y, Kim J-E, Lee J-S, Kim K-S. 2018. Metagenomic mining
439 and functional characterization of a novel KG51 bifunctional cellulase/hemicellulase from
440 black goat rumen. *Journal of agricultural and food chemistry* 66:9034-9041.
- 441 8. Yang W, Bai Y, Yang P, Luo H, Huang H, Meng K, Shi P, Wang Y, Yao B. 2015. A
442 novel bifunctional GH51 exo- α -L-arabinofuranosidase/endo-xylanase from
443 *Alicyclobacillus* sp. A4 with significant biomass-degrading capacity. *Biotechnology for*
444 *Biofuels* 8:197.
- 445 9. Malgas S, Mafa MS, Mkabayi L, Pletschke BI. 2019. A mini review of xylanolytic
446 enzymes with regards to their synergistic interactions during hetero-xylan degradation.
447 *World Journal of Microbiology and Biotechnology* 35:187.
- 448 10. Kračun SK, Schückel J, Westereng B, Thygesen LG, Monrad RN, Eijssink VGH, Willats
449 WGT. 2015. A new generation of versatile chromogenic substrates for high-throughput
450 analysis of biomass-degrading enzymes. *Biotechnology for Biofuels* 8:70.
- 451 11. Borsenberger V, Ferreira F, Pollet A, Dornez E, Desrousseaux M-L, Massou S, Courtin
452 CM, O'Donohue MJ, Fauré R. 2012. A versatile and colorful screening tool for the
453 identification of arabinofuranose-acting enzymes. *Chembiochem* 13:1885-1888.

- 454 12. Chen H-m, Armstrong Z, Hallam SJ, Withers SG. 2016. Synthesis and evaluation of a
455 series of 6-chloro-4-methylumbelliferyl glycosides as fluorogenic reagents for screening
456 metagenomic libraries for glycosidase activity. *Carbohydrate Research* 421:33-39.
- 457 13. Fonseca MJMd, Jurak E, Kataja K, Master ER, Berrin J-G, Stals I, Desmet T, Landschoot
458 AV, Briers Y. 2018. Analysis of the substrate specificity of α -L-arabinofuranosidases by
459 DNA sequencer-aided fluorophore-assisted carbohydrate electrophoresis. *Applied*
460 *Microbiology and Biotechnology* 23:10091-10102.
- 461 14. Scheller HV, Ulvskov P. 2010. Hemicelluloses. *Annual Review of Plant Biology* 61:263-
462 289.
- 463 15. Li Z, Qu H, Li C, Zhou X. 2013. Direct and efficient xylitol production from xylan by
464 *Saccharomyces cerevisiae* through transcriptional level and fermentation processing
465 optimizations. *Bioresource Technology* 149:413-419.
- 466 16. Poletto P, Pereira GN, Monteiro CRM, Pereira MAF, Bordignon SE, Oliveira Dd. 2020.
467 Xylooligosaccharides: Transforming the lignocellulosic biomasses into valuable 5-carbon
468 sugar prebiotics. *Process Biochemistry* 91:352-363.
- 469 17. Vázquez MJ, Alonso JL, Dominguez H, Parajó JC. 2001. Xylooligosaccharides:
470 manufacture and applications. *Trends in Food Science & Technology* 11:387-393.
- 471 18. Dumon C, Song L, Bozonnet S, Fauré R, O'Donohue MJ. 2012. Progress and future
472 prospects for pentose-specific biocatalysts in biorefining. *Process Biochemistry* 47:346-
473 357.
- 474 19. Wilkens C, Andersen S, Dumon C, Berrin J-g, Svensson B. 2017. GH62
475 arabinofuranosidases: Structure, function and applications. *Biotechnology Advances*
476 35:792-804.

- 477 20. Biely P, Singh S, Puchart V. 2016. Towards enzymatic breakdown of complex plant xylan
478 structures: State of the art. *Biotechnology Advances* 34:1260-1274.
- 479 21. Deutschmann R, Dekker RFH. 2012. From plant biomass to bio-based chemicals: Latest
480 developments in xylan research. *Biotechnology Advances* 30:1627-1640.
- 481 22. Kabel MA, Kortenoeven L, Schols HA, Voragen AGJ. 2002. In vitro fermentability of
482 differently substituted xylo-oligosaccharides. *Journal of agricultural and food chemistry*
483 50:6205-6210.
- 484 23. Laere KMJV, Hartemink R, Bosveld M, Schols HA, Voragen AGJ. 2000. Fermentation of
485 plant cell wall derived polysaccharides and their corresponding oligosaccharides by
486 intestinal bacteria. *Journal of agricultural and food chemistry* 48:1644-1652.
- 487 24. Holck J, Djajadi DT, Brask J, Pilgaard B, Krogh KBRM, Meyer AS, Lange L, Wilkens C.
488 2019. Novel xylanolytic triple domain enzyme targeted at feruloylated arabinoxylan
489 degradation. *Enzyme and Microbial Technology* 129:109353.
- 490 25. Lombard V, Ramulu HG, Drula E, Coutinho PM, Henrissat B. 2014. The carbohydrate-
491 active enzymes database (CAZy) in 2013. *Nucleic acids research* 42:490-495.
- 492 26. Mewis K, Lenfant N, Lombard V, Henrissat B. 2016. Dividing the large glycoside
493 hydrolase family 43 into subfamilies: A motivation for detailed enzyme characterization.
494 *Applied and Environmental Microbiology* 82:1686-1692.
- 495 27. Armstrong Z, Mewis K, Liu F, Melanie CM-I, Ming H, Kevin C, Stephen M, Hallam SJ.
496 2018. Metagenomics reveals functional synergy and novel polysaccharide utilization loci
497 in the *Castor canadensis* fecal microbiome. *The ISME Journal* 12:2757-2769.
- 498 28. Jiménez-Ortega E, Valenzuela S, Ramírez-Escudero M, Pastor FJ, Sanz-Aparicio J. 2020.
499 Structural analysis of the reducing-end xylose-releasing exo-oligoxyylanase Rex8A from
500 *Paenibacillus barcinonensis* BP-23 deciphers its molecular specificity. *The FEBS Journal*.

- 501 29. Valenzuela SV, Lopez S, Biely P, Sanz-Aparicio J, Pastor FIJ. 2016. The glycoside
502 hydrolase family 8 reducing-end xylose-releasing exo-oligoxyranase Rex8A from
503 *Paenibacillus barcinonensis* BP-23 is active on branched xylooligosaccharides. *Applied*
504 *and Environmental Microbiology* 82:5116–5124.
- 505 30. Rio TGD, Abt B, Spring S, Lapidus A, Nolan M, Tice H, Copeland A, Cheng J-F, Chen
506 F, Bruce D, Goodwin L, Pitluck S, Ivanova N, Mavromatis K, Mikhailova N, Pati A,
507 Chen A, Palaniappan K, Land M, Hauser L, Chang Y-J, Jeffries CD, Chain P, Saunders E,
508 Detter JC, Brettin T, Rohde M, Göker M, Bristow J, Eisen JA, Markowitz V, Hugenholtz
509 P, Kyrpides NC, Klenk H-P, Lucas S. 2010. Complete genome sequence of *Chitinophaga*
510 *pinensis* type strain (UQM 2034T). *Standards in Genomic Sciences* 2:87-95.
- 511 31. Teeravivattanakit T, Baramée S, Phitsuwan P, Waeonukul R, Pason P, Tachaapaikoon C,
512 Sakka K, Ratanakhanokchai K. 2016. Novel trifunctional xylanolytic enzyme Axy43A
513 from *Paenibacillus curdolanolyticus* strain B-6 exhibiting endo-xylanase, beta-D-
514 xylosidase, and arabinoxylan arabinofuranohydrolase activities. *Applied and*
515 *Environmental Microbiology* 82:6942-6951.
- 516 32. Broberg A, Duus J, Thomsen KK, Ferre H. 2000. A novel type of arabinoxylan
517 arabinofuranohydrolase isolated from germinated barley analysis of substrate preference
518 and specificity by nano-probe NMR. *European Journal of Biochemistry* 267:6633-6641.
- 519 33. Mathieu SV, Aragão KS, Imberty A, Varrot A. 2010. Discoidin I from *Dictyostelium*
520 *discoideum* and interactions with oligosaccharides: specificity, affinity, crystal structures
521 and comparison with Discoidin II. *Journal of Molecular Biology* 400:540-554.
- 522 34. Vincent P, Shareck F, Dupont C, Morosoli R, Kluepfel D. 1997. New α -L-
523 arabinofuranosidase produced by *Streptomyces lividans*: cloning and DNA sequence of
524 the abfB gene and characterization of the enzyme. *Biochemical Journal* 322:845-852.

- 525 35. Adelsberger H, Hertel C, Glawischnig E, Zverlov VV, Schwarz WH. 2004. Enzyme
526 system of *Clostridium stercorarium* for hydrolysis of arabinoxylan: reconstitution of the
527 *in vivo* system from recombinant enzymes. *Microbiology* 150:2257-2266.
- 528 36. Saha BC. 2003. Hemicellulose bioconversion. *Industrial Biotechnology Journal* 30:279-
529 291.
- 530 37. Lagaert S, Pollet A, Delcour JA, Lavigne R, Courtin CM, Volckaert G. 2011.
531 Characterization of two β -xylosidases from *Bifidobacterium adolescentis* and their
532 contribution to the hydrolysis of prebiotic xylooligosaccharides. *Applied Microbiology*
533 *and Biotechnology* 92:1179-1185.
- 534 38. Honda Y, Kitaoka M. 2004. A family 8 glycoside hydrolase from *Bacillus halodurans* C-
535 125 (BH2105) is a reducing end xylose-releasing exo-oligoxyylanase. *The Journal of*
536 *biological chemistry* 279:55097–55103.
- 537 39. Lagaert S, Campenhout SV, Pollet A, Bourgois TM, Delcour JA, Courtin CM, Volckaert
538 G. 2007. Recombinant expression and characterization of a reducing-end xylose-releasing
539 exo-oligoxyylanase from *Bifidobacterium adolescentis*. *Applied and Environmental*
540 *Microbiology* 73:5374-5377.
- 541 40. Hong P-Y, Iakiviak M, Dodd D, Zhang M, Mackie RI, Canna I. 2014. Two new xylanases
542 with different substrate specificities from the human gut bacterium *Bacteroides*
543 *intestinalis* DSM 17393. *Applied and Environmental Microbiology* 80:2084-2093.
- 544 41. Lagaert S, Pollet A, Courtin CM, Volckaert G. 2014. β -Xylosidases and α -L-
545 arabinofuranosidases: accessory enzymes for arabinoxylan degradation. *Biotechnology*
546 *Advances* 32:316-332.



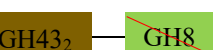


- 547 42. Amorim C, Silvério SC, Prather KLJ, Rodrigues LR. 2019. From lignocellulosic residues
548 to market: Production and commercial potential of xylooligosaccharides. *Biotechnology*
549 *Advances* 37:107397.
- 550 43. Wongratpanya K, Imjongjairak S, Waonukul R, Sornyotha S, Phitsuwan P, Pason P,
551 Nimchua T, Tachaapaikoon C, Ratanakhanokchai K. 2015. Multifunctional properties of
552 glycoside hydrolase family 43 from *Paenibacillus curdlanolyticus* strain B-6 including
553 exo-beta-xylosidase, endoxylanase, and alpha-L-arabinofuranosidase activities.
554 *Bioresources* 10:2492-2505.
- 555 44. Broeker J, Mechelke M, Baudrexl M, Mennerich D, Hornburg D, Mann M, Schwarz WH,
556 Liebl W, Zverlov VV. 2018. The hemicellulose-degrading enzyme system of the
557 thermophilic bacterium *Clostridium stercorarium*: comparative characterisation and
558 addition of new hemicellulolytic glycoside hydrolases. *Biotechnology for Biofuels*
559 11:229.
- 560 45. Wang Y, Sakka M, Yagi H, Kaneko S, Katsuzaki H, Kunitake E, Kimura T, Sakka K.
561 2018. *Ruminiclostridium josui* Abf62A-Axe6A: A tri-functional xylanolytic enzyme
562 exhibiting α -L-arabinofuranosidase, endoxylanase, and acetylxyylan esterase activities.
563 *Enzyme and Microbial Technology* 117:1-8.
- 564 46. Bachmann SL, McCarthy AJ. 1991. Purification and cooperative activity of enzymes
565 constituting the xylan-degrading system of *Thermomonospora fusca*. *Applied and*
566 *Environmental Microbiology* 57:2121-2130.
- 567 47. Huang Y, Zheng X, Pilgaard B, Holck J, Muschiol J, Li S, Lange L. 2019. Identification
568 and characterization of GH11 xylanase and GH43 xylosidase from the chytridiomycetous
569 fungus, *Rhizophlyctis rosea*. *Applied Microbiology and Biotechnology* 103:777-791.

- 570 48. Rohman A, Oosterwijk Nv, Puspaningsih NNT, Dijkstra BW. 2018. Structural basis of
571 product inhibition by arabinose and xylose of the thermostable GH43 β -1,4-xylosidase
572 from *Geobacillus thermoleovorans* IT-08. PloS ONE 13:e0196358.
- 573 49. Schaeper JP, Sepaniak MJ. 2000. Parameters affecting reproducibility in capillary
574 electrophoresis. Electrophoresis 21:1421-1429.
- 575 50. Fauré R, Courtin CCM, Delcour DJA, Dumon DC, Faulds CCB, Geoffrey EB, Fort FS,
576 Fry GSC, Halila HS, Kabel GMA, Pouvreau L, Bernard I, Rivet JA, Saulnier GL, Schols
577 JHA, Driguez IH, A MJOD. 2009. A brief and informationally rich naming system for
578 oligosaccharide motifs of heteroxylans found in plant cell walls. Australian Journal of
579 Chemistry 62:533-537.
- 580
581
582
583
584
585
586
587
588
589
590
591
592
593

594 **Tables**

595

596 **Table 1 - Metagenomic AX-active enzymes analyzed in this study.** The CAZy family (and
 597 subfamily in subscript) is given for the modules that constitute each enzyme. Domains
 598 inactivated by mutagenesis are indicated with a red line. Activity tests on aryl glycosides p-
 599 nitrophenyl β -D-xylopyranoside (pNP-X), 4-methylumbelliferyl β -D-xylopyranoside (MU-X), 6-
 600 chloro-4-methylumbelliferyl β -D-xylopyranoside (CMU-X), p-nitrophenyl α -L-
 601 arabinofuranoside (pNP-Ara) and 4-methylumbelliferyl α -L-arabinofuranoside (MU-Ara) and
 602 HPAEC-PAD analysis using A³X, A²XX, XA³XX and XA²XX as substrates were performed by
 603 (27). CBM = Carbohydrate binding module. Rex = reducing end xylose-releasing exo-
 604 oligoxylanase.

| Protein name used in this study | Protein name used in (27) | Enzyme modularity | Activity on aryl glycosides | Activity detected by HPAEC-PAD | Observations |
|---------------------------------|---------------------------|---|-----------------------------|---|--|
| MG43 ₂₈ | 12_J03-18 |  | CMU-X | Not tested | - |
| MG43 ₂₋₈ | 12_H03-13 |  | CMU-X | Rex and β -xylosidase | Does not hydrolyse X ₂ |
| MG43 ₂ | 12_H03-13_E507A |  | CMU-X | β -xylosidase | Does not hydrolyse X ₂ |
| MG8 | 12_H03-13_E209A |  | Not detected | Rex | - |
| MG43 ₇ | 12_H03-12 |  | Not detected | Cleaves O-3-arabinose decorations from A ³ X | Only active in the presence of MG43 ₂₋₈ |

605

606 **Table 2 - Expression conditions of the metagenome-derived enzymes studied in this work.**

| Enzyme | Expression host | Host growth temperature | Induction type | Purification method |
|---------------------|-------------------------------------|--|--|--|
| MG43 ₂₈ | <i>E. coli</i> BL21 (DE3) | 24 h at 37 °C, 250 rpm on LBE50-52 auto-induction medium | | HisGraviTrap |
| MG43 ₂₋₈ | <i>E. coli</i> BL21 CodonPlus (DE3) | 37 °C, 250 rpm | 1 mM IPTG at 16 °C for 18 to 20 hours, 250 rpm | HisPur Ni-NTA Superflow agarose (250/100 µL resin) |
| | <i>E. coli</i> ArcticExpress | 30 °C, 250 rpm | 1 mM IPTG at 16 °C for 24 hours, 250 rpm | HisPur Ni-NTA Superflow agarose (100 µL resin) |
| MG43 ₂ | <i>E. coli</i> BL21 CodonPlus (DE3) | 30 °C/37 °C, 250 rpm | 1 mM IPTG at 16 °C for 18 to 20 hours, 250 rpm | HisPur Ni-NTA Superflow agarose (500/100 µL resin) |
| MG43 ₇ | | 18 h at 30 °C, 250 rpm on LBE50-52 auto-induction medium | | HisGraviTrap |
| | | 30 °C, 250 rpm | 1 mM IPTG at 16 °C for 18 hours, 250 rpm | HisPur Ni-NTA Superflow agarose (500 µL resin) |
| MG8 | <i>E. coli</i> BL21 (DE3) | 37 °C, 250 rpm | 1 mM IPTG at 16 °C for 18 hours, 250 rpm | HisPur Ni-NTA Superflow agarose (500 µL resin) |

607

608

609

610

611

612

613

614

615

616

617 **Figures**

618

619

620

621

622

623

624

625

626

627

628

629

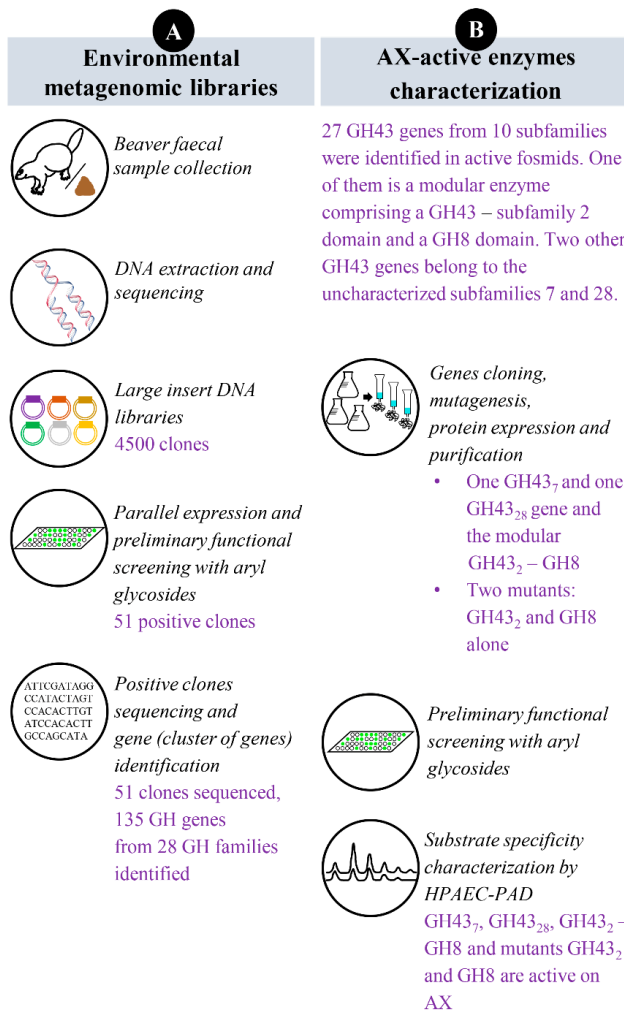
630

631

632

633

634

635 **Figure 1 – Preceding functional screening of putative enzymes derived from metagenomics**636 **on beaver fecal samples.** A) Upon environmental sample collection and gDNA extraction, a

637 metagenomic DNA library of 4500 clones suitable for heterologous expression was constructed.

638 These clones were expressed and checked for active hits by high-throughput preliminary

639 functional screening methods. Fifty one active hits were sequenced and 135 putative glycoside

640 hydrolases (GHs) from 28 GH families were identified by in silico analysis. B) Three GH43

29

641 genes, one of which is modular with an additional GH8 domain, and two mutants thereof were
642 characterized by enzymatic activity tests with aryl glycosides and by HPAEC-PAD using
643 representative arabinoxylan oligosaccharides (27).

644

645

646

647

648

649

650

651

652

653

654

655

656

657

658

659

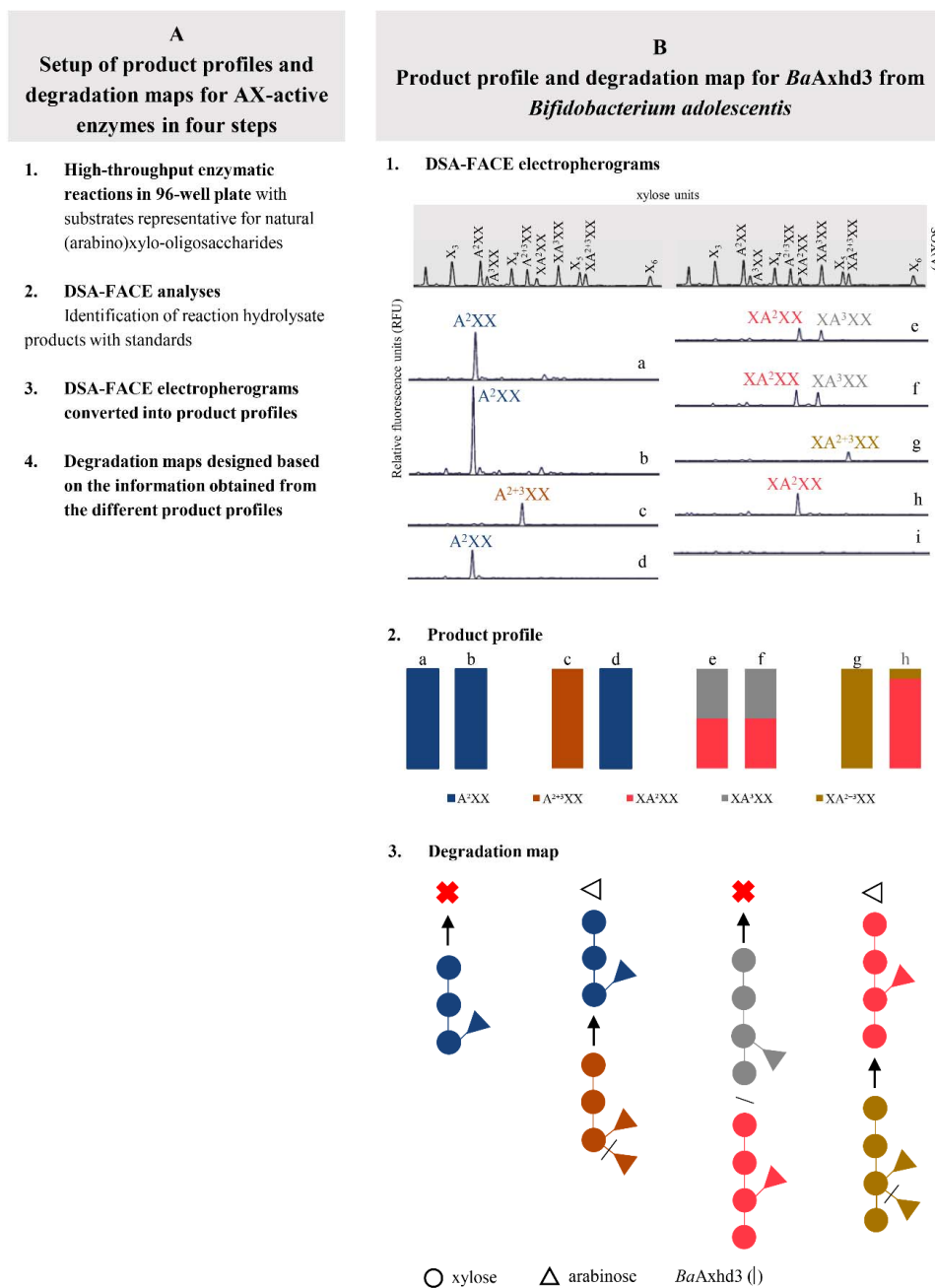
660

661

662

663

664



665 **Figure 2 – Product profiles and degradation maps.** (A) General approach to establish DSA-
 666 FACE product profiles and a corresponding degradation map in four steps. (B) Product profiles

31

667 for *BaAxhd3* from *Bifidobacterium adolescentis* after reaction with A^2XX , $A^{2+3}XX$, XA^2XX ,
668 XA^3XX and $XA^{2+3}XX$. Electropherograms a, c, e and g show the substrate blanks, whereas
669 electropherograms b, d, f and h show the corresponding hydrolysates upon enzymatic reaction
670 with *BaAxhd3*. The peaks are compared to standards for carbohydrate peaks identification (1). A
671 qualitative interpretation of the electropherograms is then displayed on a product profile (bars are
672 labeled with the letters of corresponding electropherograms) (2). Substrate conversions are easily
673 observed by a color change. The first bar corresponds to the substrate blank followed by bar(s)
674 showing colors corresponding to the (A)XOS found upon enzymatic reaction. A degradation map
675 is obtained from the different product profiles for *BaAxhd3* (3).

676

677

678

679

680

681

682

683

684

685

686

687

688
689
690
691
692
693
694
695
696
697
698
699
700
701
702
703
704
705
706
707
708
709
710

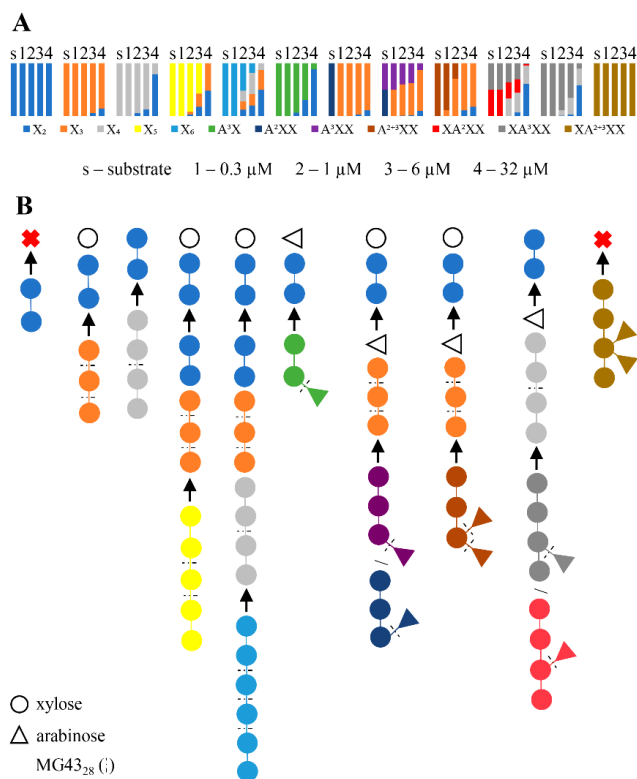


Figure 3 - Product profiles starting from 12 (A)XOS and degradation map of MG43₂₈. The product profiles (A) show the hydrolysis products obtained after 22 h of enzymatic reactions with 0.3, 1, 6 and 32 μM MG43₂₈ (1, 2, 3 and 4 respectively). The (A)XOS used as substrates for the enzymatic reactions are identified as 's'. A degradation map is given in B with a schematic representation of the (A)XOS structures used as substrates and the ones obtained as hydrolysis products, using corresponding colors. Based on hydrolysis products obtained, cleavage positions for MG43₂₈ are indicated with \downarrow .

711
712
713
714
715
716
717
718
719
720
721
722
723
724
725
726
727
728
729
730
731
732

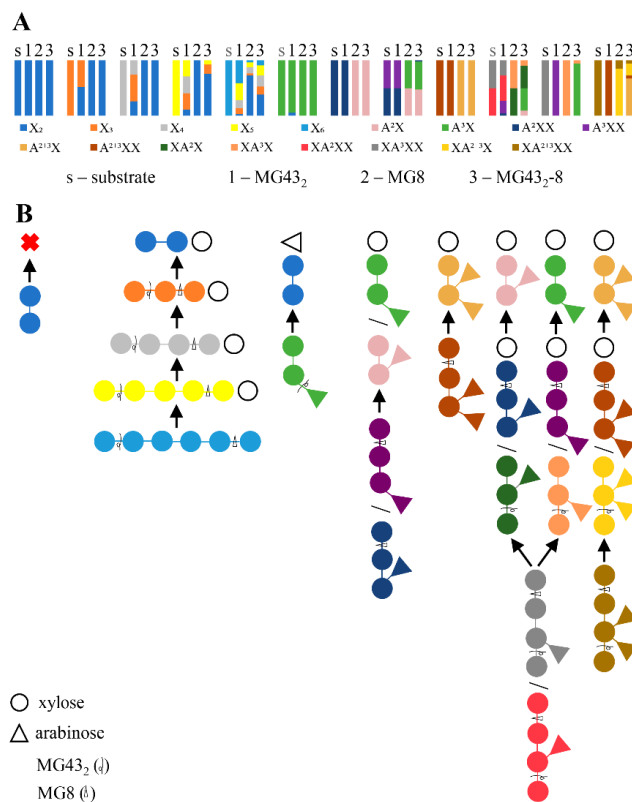
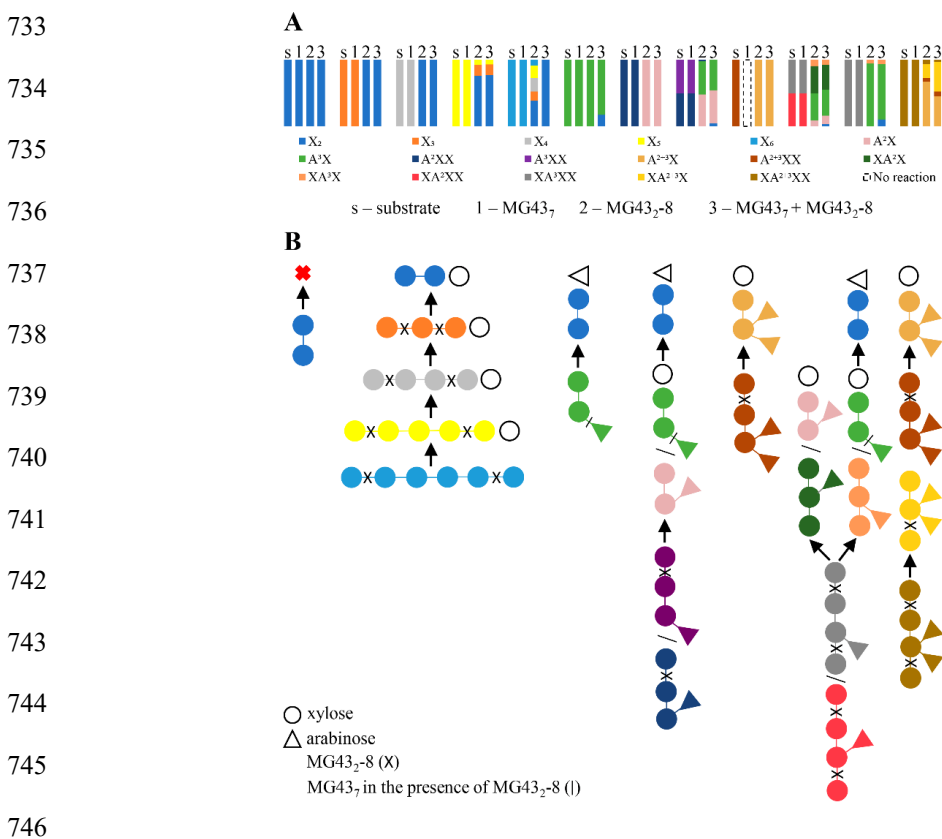


Figure 4 - Product profiles of MG43₂, MG8 and MG43₂-8. The product profiles in A show the hydrolysis products obtained after 22 h of enzymatic reactions with 3 μ M MG43₂ (1), MG8 (2) and MG43₂-8 (3). The (A)XOS used as substrates for the enzymatic reactions are identified as 's'. A degradation map is given in B with a schematic representation of the (A)XOS structures used as substrates and the ones obtained as hydrolysis products, using corresponding colors. Based on hydrolysis products obtained, cleavage positions for MG43₂ and MG8 are indicated with \dagger and $\hat{\Delta}$, respectively.



747 **Figure 5 - Product profiles of MG43₇, MG43₂₋₈, and MG43₇ in the presence of MG43₂₋₈.** The

748 product profiles (A) show the hydrolysis products obtained after 22 h of enzymatic reactions with

749 8 μM MG43₇ (1), 3 μM MG43₂₋₈ (2) and 8 μM MG43₇ in the presence of 3 μM MG43₂₋₈ (3).

750 The (A)XOS used as substrates for the enzymatic reactions are identified as 's'. The dotted line

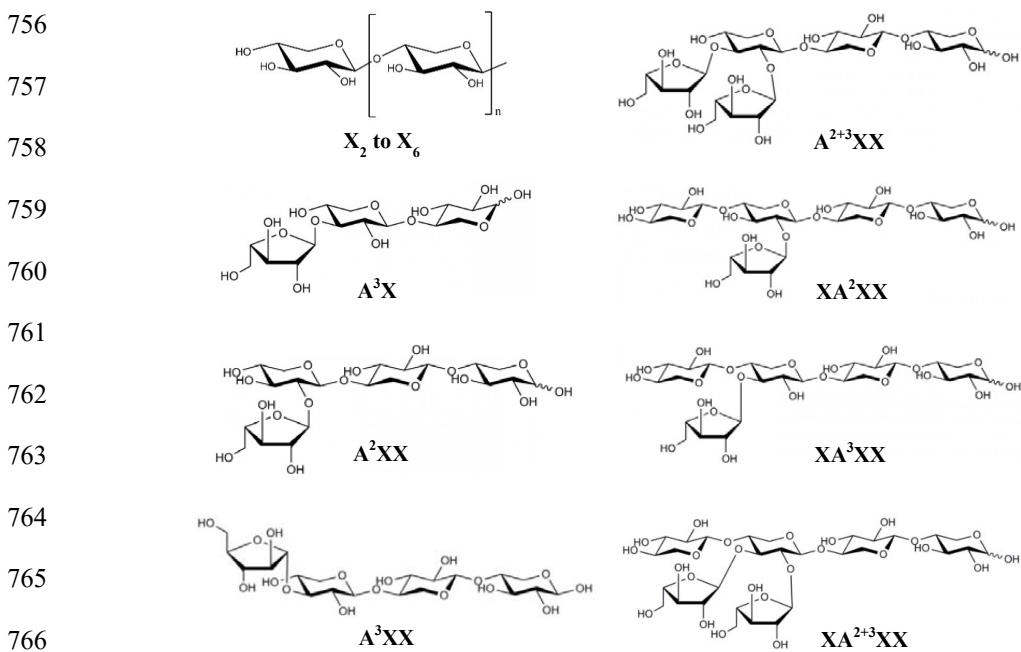
751 means there was no reaction performed to test the hydrolysis of A²⁺³XX by MG43₇. A

752 degradation map is given in B with a schematic representation of the (A)XOS structures used as

753 substrates and the ones obtained as hydrolysis products. Based on hydrolysis products obtained,

754 cleavage positions for MG43₇ and MG43₂₋₈ are indicated with l and x, respectively.

755



767 **Figure 6 - Twelve different (arabino)xylo-oligosaccharides ((A)XOS) used as substrates in**
 768 **the enzymatic reactions and as standards for the DSA-FACE analysis. AXOS are named**
 769 **according to nomenclature proposed by (50).**

770

771

772

773

774

775

776

777

778

779

780

781

782

783

784

785

786

787

788

789

790

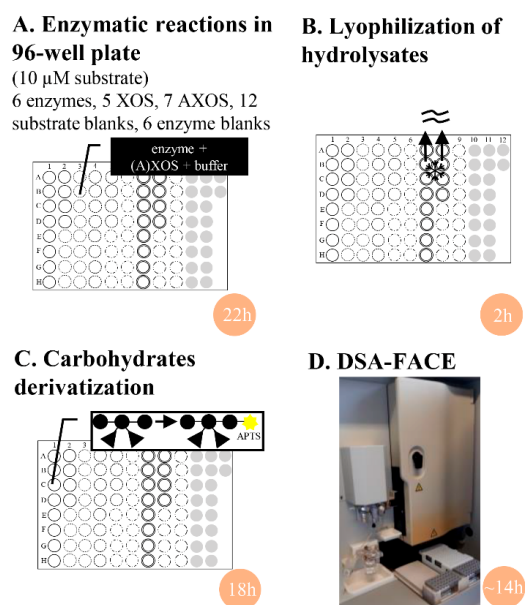
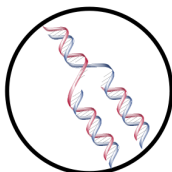
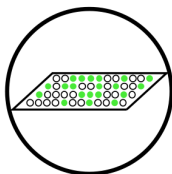
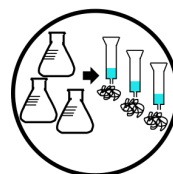


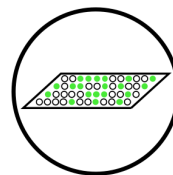
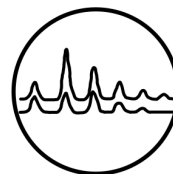
Figure 7 - Protocol for high-throughput study of substrate specificities of arabinoxylan-active enzymes by DSA-FACE. Putative AX-active enzymes are incubated with (A)XOS for 22 hours (A). Six enzymes were tested against 12 (A)XOS, including 12 substrate blanks and 6 enzyme blanks (90 samples in total). Reaction hydrolysates are then diluted with ultrapure water and lyophilized (B). Afterwards, reductive amination reactions are performed to derivatize the carbohydrates at their reducing end with the negatively charged and fluorescent APTS (C). Ten microliters of derivatized reaction hydrolysate are analyzed by DSA-FACE (D). All steps are done in a 96-well plate and 90 samples are analyzed in approximately 14 hours.

A**Environmental
metagenomic libraries***Beaver faecal
sample collection**DNA extraction and
sequencing**Large insert DNA
libraries
4500 clones**Parallel expression and
preliminary functional
screening with aryl
glycosides
51 positive clones*ATTCGATAGG
CCATACTAGT
CCACACTTGT
ATCCACACTT
GCCAGCATA*Positive clones
sequencing and
gene (cluster of genes)
identification
51 clones sequenced,
135 GH genes
from 28 GH families
identified***B****AX-active enzymes
characterization**

27 GH43 genes from 10 subfamilies were identified in active fosmid. One of them is a modular enzyme comprising a GH43 – subfamily 2 domain and a GH8 domain. Two other GH43 genes belong to the uncharacterized subfamilies 7 and 28.

*Genes cloning,
mutagenesis,
protein expression and
purification*

- One GH43₇ and one GH43₂₈ gene and the modular GH43₂ – GH8
- Two mutants: GH43₂ and GH8 alone

*Preliminary functional
screening with aryl
glycosides**Substrate specificity
characterization by
HPAEC-PAD*

GH43₇, GH43₂₈, GH43₂ – GH8 and mutants GH43₂ and GH8 are active on AX

A

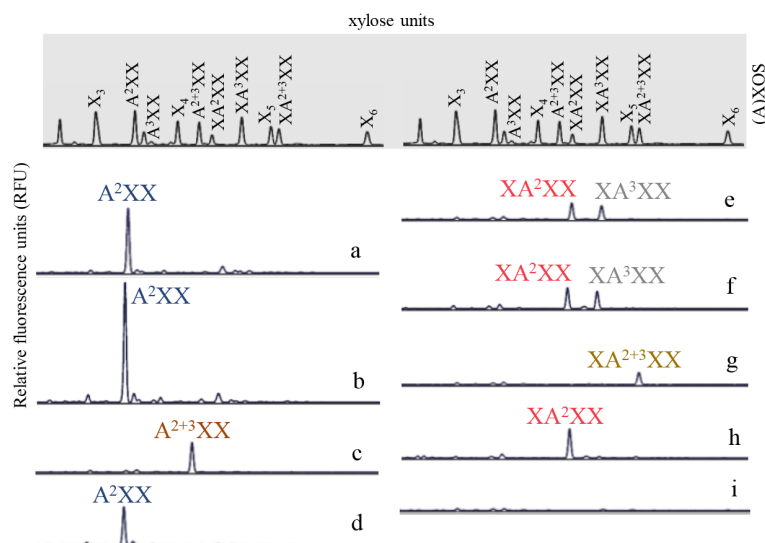
Setup of product profiles and degradation maps for AX-active enzymes in four steps

1. High-throughput enzymatic reactions in 96-well plate with substrates representative for natural (arabino)xylo-oligosaccharides
2. DSA-FACE analyses
Identification of reaction hydrolysate products with standards
3. DSA-FACE electropherograms converted into product profiles
4. Degradation maps designed based on the information obtained from the different product profiles

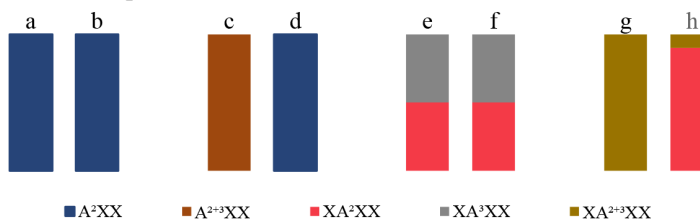
B

Product profile and degradation map for *BaAxhd3* from *Bifidobacterium adolescentis*

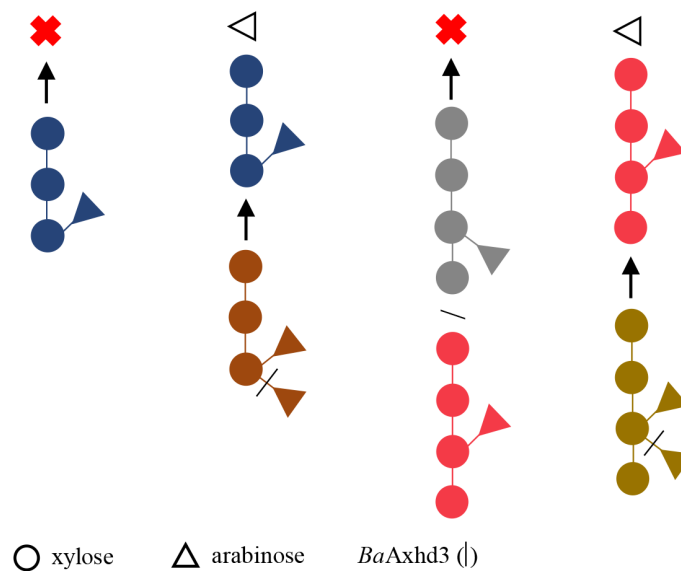
1. DSA-FACE electropherograms

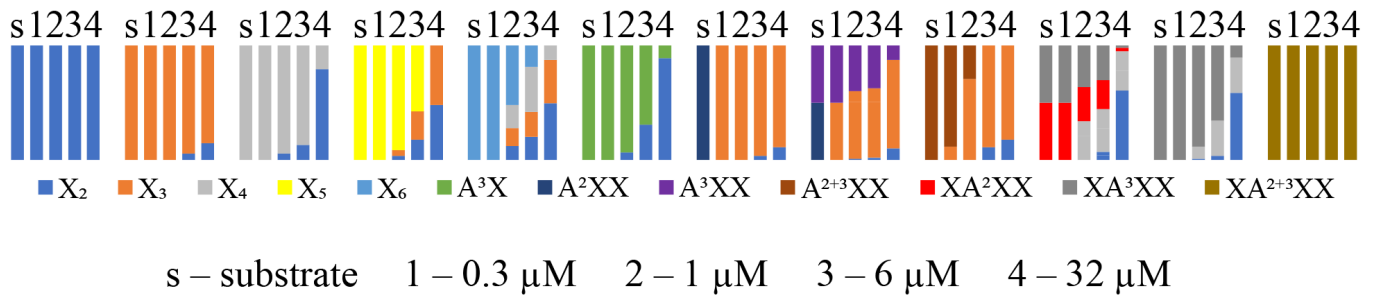
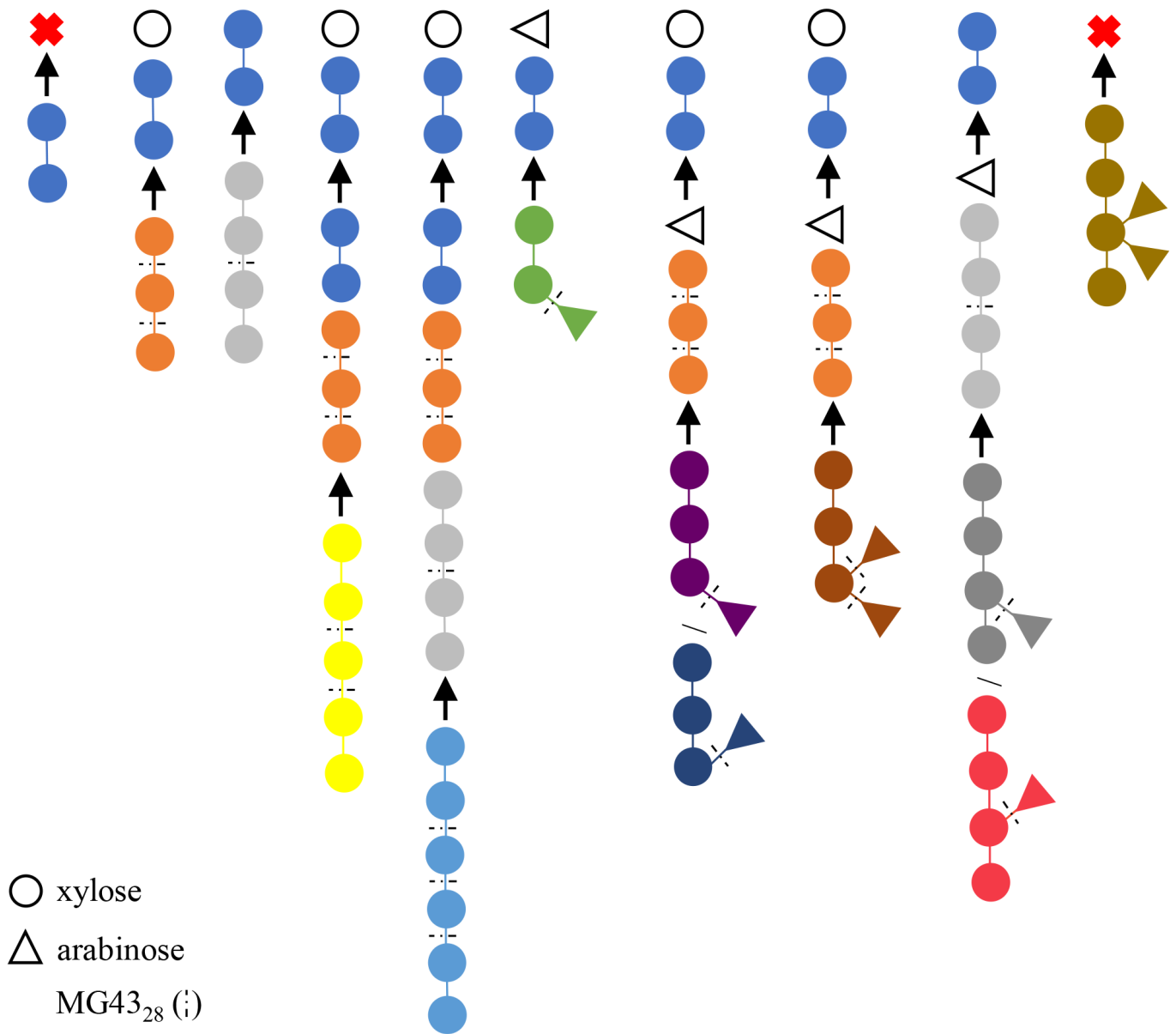


2. Product profile

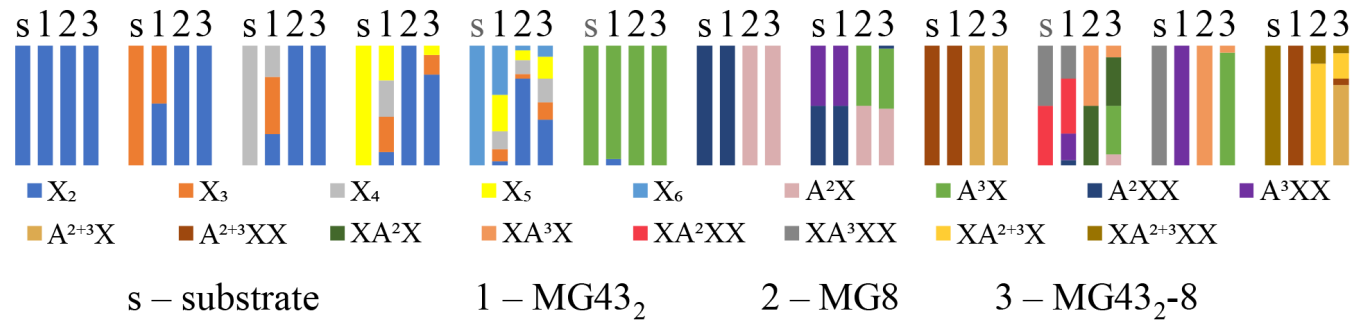


3. Degradation map

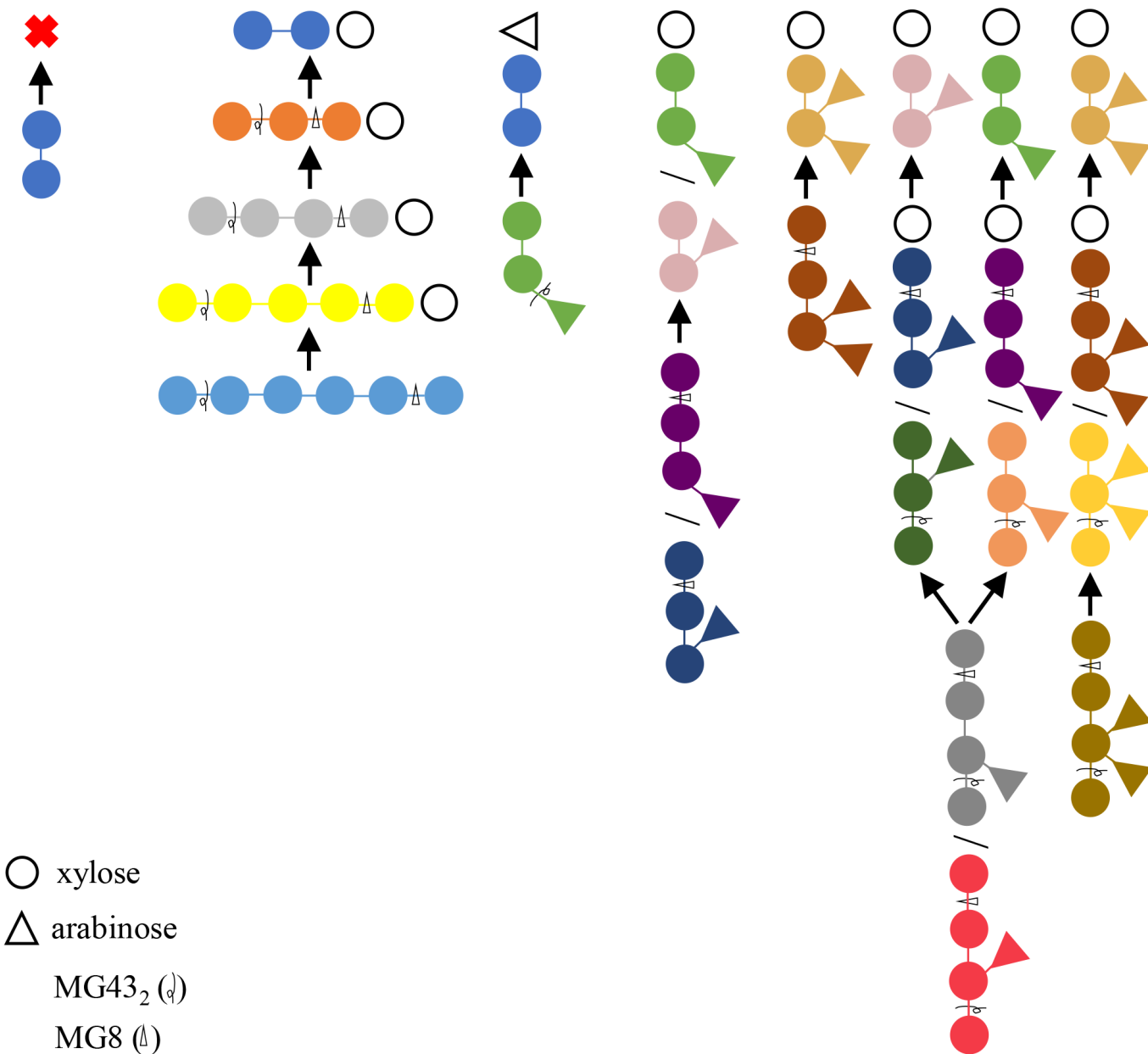


A**B**

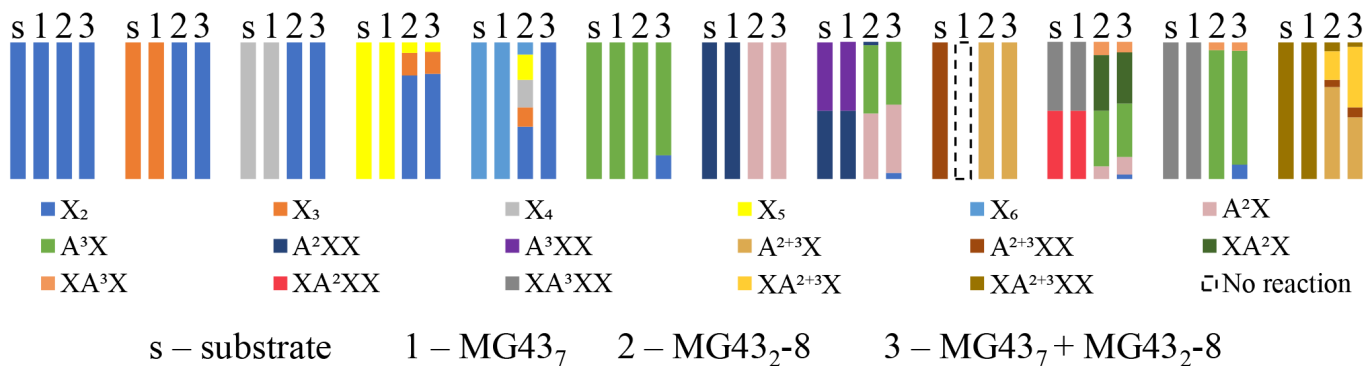
A



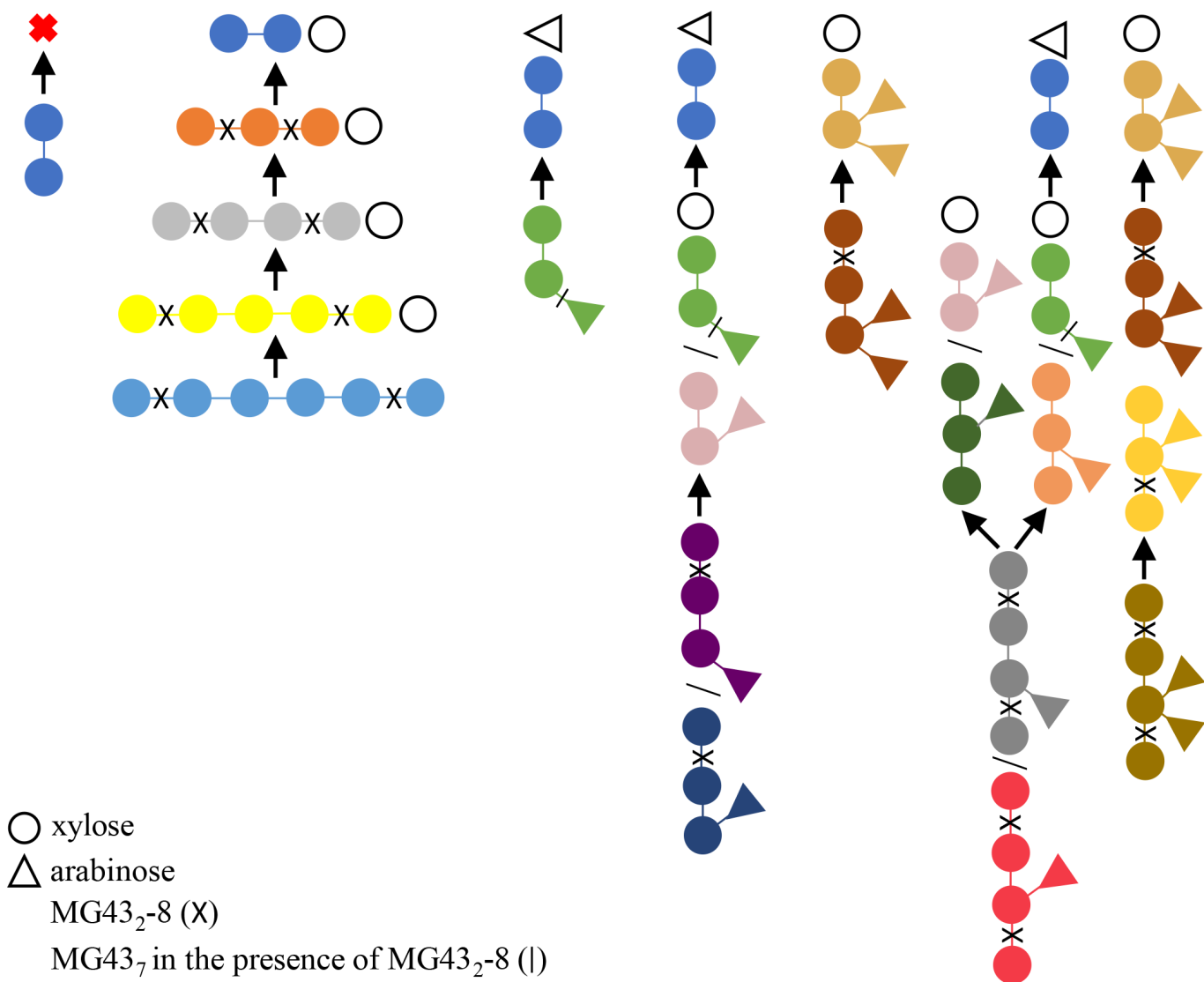
B

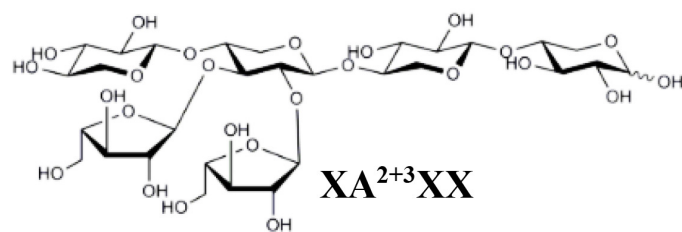
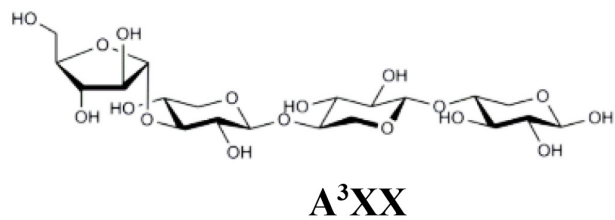
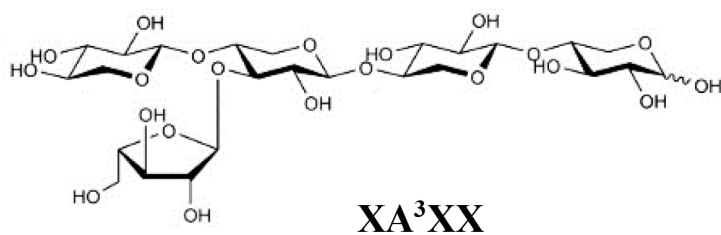
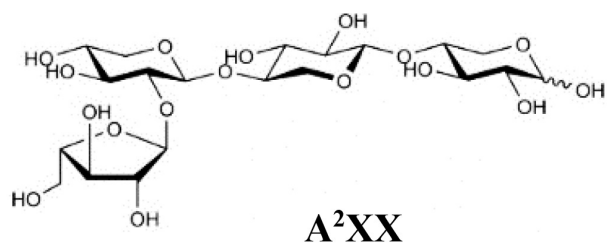
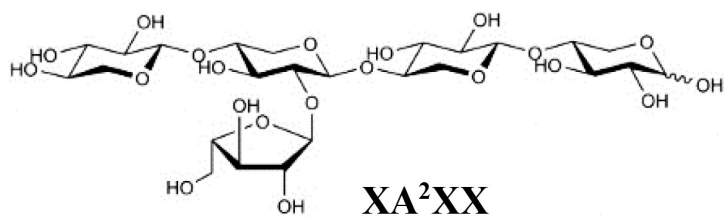
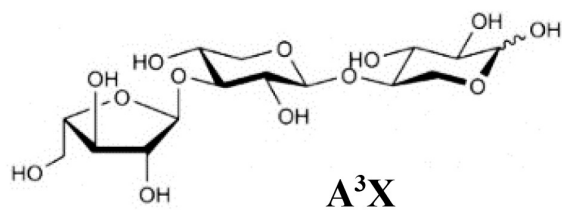
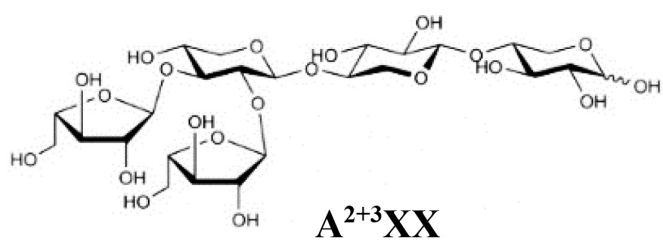
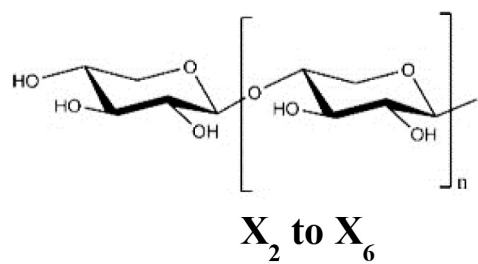


A



B

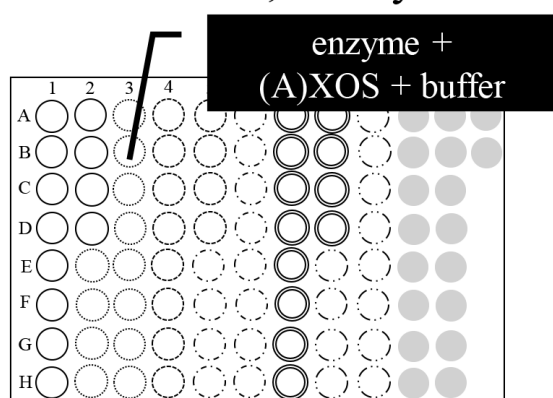




A. Enzymatic reactions in 96-well plate

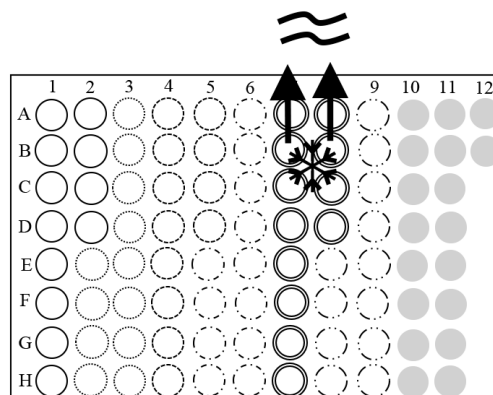
(10 μ M substrate)

6 enzymes, 5 XOS, 7 AXOS, 12 substrate blanks, 6 enzyme blanks



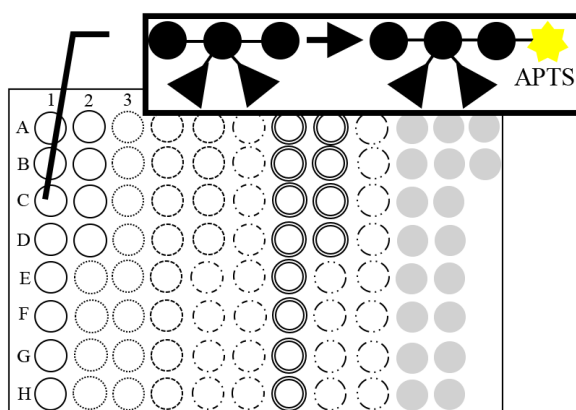
22h

B. Lyophilization of hydrolysates



2h

C. Carbohydrates derivatization



18h

D. DSA-FACE



~14h